ORIGINAL ARTICLE

Astaxanthine attenuates cisplatin ototoxicity *in vitro* and protects against cisplatin-induced hearing loss *in vivo*

Benyu Nan[a,b,†], Zirui Zhao[c,†], Kanglun Jiang[a], Xi Gu[d,*], Huawei Li[e,f,g,h,*], Xinsheng Huang[a,*]

[a]Department of Otorhinolaryngology-Head and Neck Surgery, Zhongshan Hospital, Fudan University, Shanghai 200030, China
[b]Department of Otorhinolaryngology-Head and Neck Surgery, Wenzhou Medical University, Affiliated Hospital 2, Wenzhou 325000, China
[c]Department of Otolaryngology, Yueyang Hospital of Integrated Traditional Chinese and Western Medicine, Shanghai University of Traditional Chinese Medicine, Shanghai 200437, China
[d]Department of Otolaryngology, the First Affiliated Hospital of Fujian Medical University, Fuzhou 350005, China
[e]ENT Institute and Department of Otorhinolaryngology, Eye & ENT Hospital, State Key Laboratory of Medical Neurobiology and MOE Frontiers Center for Brain Science, Fudan University, Shanghai 200031, China
[f]Institutes of Biomedical Sciences, Fudan University, Shanghai 200032, China
[g]NHC Key Laboratory of Hearing Medicine (Fudan University), Shanghai 200031, China
[h]The Institutes of Brain Science and the Collaborative Innovation Center for Brain Science, Fudan University, Shanghai 200032, China

Abstract Astaxanthine (AST) has important biological activities including antioxidant and anti-inflammatory effects that could alleviate neurological and heart diseases, but its role in the prevention of cisplatin-induced hearing loss (CIHL) is not yet well understood. In our study, a steady interaction between AST and the E3 ligase adapter Kelch-like ECH-associated protein 1, a predominant repressor of nuclear factor erythroid 2-related factor 2 (NRF2), was performed and tested *via* computer molecular docking and dynamics. AST protected against cisplatin-induced ototoxicity *via* NRF2 mediated pathway

*Corresponding authors. Tel.: +86 591 87982117, fax: +86 591 87982117 (Xi Gu); Tel.: +86 21 64377134 669, fax: +86 21 64377151 (Huawei Li); Tel.: +86 21 64041990, fax: +86 21 64041990 (Xinsheng Huang).

E-mail addresses: harry-xixi@hotmail.com (Xi Gu), hwli@shmu.edu.cn (Huawei Li), huang.xinsheng@zs-hospital.sh.cn (Xinsheng Huang).

†These authors made equal contributions to this work.

using quantitative PCR and Western blotting. The levels of reactive oxygen species (ROS) and mitochondrial membrane potential revealed that AST reduced ROS overexpression and mitochondrial dysfunction. Moreover, AST exerted anti-apoptosis effects in mouse cochlear explants using immunofluorescence staining and HEI-OC1 cell lines using quantitative PCR and Western blotting. Finally, AST combined with poloxamer was injected into the middle ear through the tympanum, and the protection against CIHL was evaluated using the acoustic brain stem test and immunofluorescent staining in adult mice. Our results suggest that AST reduced ROS overexpression, mitochondrial dysfunction, and apoptosis *via* NRF2-mediated pathway in cisplatin-exposed HEI-OC1 cell lines and mouse cochlear explants, finally promoting cell survival. Our study demonstrates that AST is a candidate therapeutic agent for CIHL.

1. Introduction

It is known that hearing impairment can be triggered by a diversity of possibilities including noise exposure, viral infection, and ototoxic chemicals such as platinum-containing agents, loop diuretics, and aminoglycoside antibiotics[1,2]. Cisplatin-associated ototoxicity, which is permanent and mostly bilateral, has debilitating effects on education development and psychosocial integration, especially in children[3−6]. Previous studies which investigated the cisplatin ototoxicity reported that accumulation of cisplatin in the organ of Corti, the stria vascularis, and spiral ganglion neurons was mainly regulated by passive diffusion and various transportation channels[7−12]. Since accumulation of cisplatin-induced reactive oxygen species (ROS) promotes inflammation, protein nitration, lipid peroxidation and DNA damage, there exists a critical strategy for maintaining hair cells (HCs) after cisplatin exposure, which is preventing auditory cell from apoptosis *via* managing excessive ROS generation[13,14].

Astaxanthine (AST), the main oceanic carotenoid pigment produced in marine animals, presents stronger antioxidant activity and polar properties than other carotenoids because of the presence of hydroxyl and keto groups on both ends of the molecule (Fig. 1A)[15,16]. Because of its unique molecular properties, AST can maintain the integrity of the cellular membranes and mitochondrial function by stretching through bilayers and diminishing ROS distributed in both the inner and outer layers[17,18]. Previous studies showed that AST protected against cisplatin-induced hearing loss (CIHL) at high frequencies in rats and neomycin-induced lateral-line HC death in zebra fish[19,20]. It is suggested that the antioxidant activity of AST is associated with several potential mechanisms, including the activation of MAPK, nuclear factor erythroid 2-related factor 2 (NRF2)/antioxidant response element (ARE), and PI3K/AKT pathways[21−23].

As a redox-sensitive nuclear factor, NRF2 plays a vital role in the cellular antioxidant self-defense system mainly *via* regulating ARE transcriptional activation to protect organs from oxidative stress[24−26]. Under non-stressed conditions, only low NRF2 is constitutively expressed by cells as degraded by ubiquitination, which ensures a cellular prompt protective response to oxidative, metabolic stress, and inflammation. The stability of NRF2 is mainly regulated by the E3 ligase adapter Kelch-like ECH-associated protein 1 (KEAP1) which is a homodimer protein comprising of three functional domains (Fig. 1B)[27]. It has been shown that the NRF2−ARE pathway is involved in other antioxidants or chemicals against CIHL[28,29].

Molecular docking, as a computer-aided prediction of optimal docking between molecules, is universally applied in the fields of structural molecular biology and pharmaceutical drug design, which can determine the correct conformational space within small molecules and calculate the strength of the protein−ligand interactions[30]. As for drug discovery, molecular docking and molecular dynamics (MD) play vital roles in the virtual screening and design of new bioactive molecules[31,32].

It was shown that AST could regulate the NRF2/ARE pathway to inhibit oxidative stress response in the neurogenic disease[33]. AST has a similar molecular structure to β-carotene that is a selective NRF2 activator, but much stronger antioxidant ability than that of β-carotene[34]. Therefore, we hypothesized that AST could compete with NRF2 for KEAP1 binding, leading to dissociation of NRF2 and translocation to the nucleus, promoting the downstream antioxidant factors. First, we successfully bound the astaxanthine molecule to KEAP1 *via* molecular docking. MD was applied to analyze the stability of the binding complex. Next, we confirmed that AST protects against cisplatin-induced ototoxicity *via* NRF2 mediated pathway. It was found that AST reduced ROS overexpression, mitochondrial dysfunction, and apoptosis both in the House Ear Institute-Organ of Corti 1 (HEI-OC1) cell line and the mouse cochlear explants following cisplatin treatment. Finally, our study demonstrates that astaxanthine is a candidate therapeutic agent for CIHL without compromising cisplatin antitumor efficacy.

2. Materials and methods

2.1. Molecular docking and dynamics simulation

The docking study of the compound [AST, protein data bank (PDB) ID: AXT] and target (KEAP1, PDB ID: 6LRZ) was performed with AutoDock 4.2 (the Scripps Research Institute, La Jolla, San Diego, CA, USA). The BIOVIA Discovery Studio 2017 (Dassault Systèmes, San Diego, CA, USA) was used for preprocessing the chemical structure and biomolecules. The Lamarckian genetic algorithm was employed to search for docking information. During the docking procedure, the key residues in the binding pocket were kept flexible. The center of the target binding pocket was determined as the grid placement. All runs were subjected to 2.5 million rounds of energy evaluation steps. The representative pose selection was performed based on a cluster analysis of the docked poses. The *PyMOL* Molecular Graphics System Version 1.8.4.0 (DeLano Scientific LLC, Palo Alto, CA,
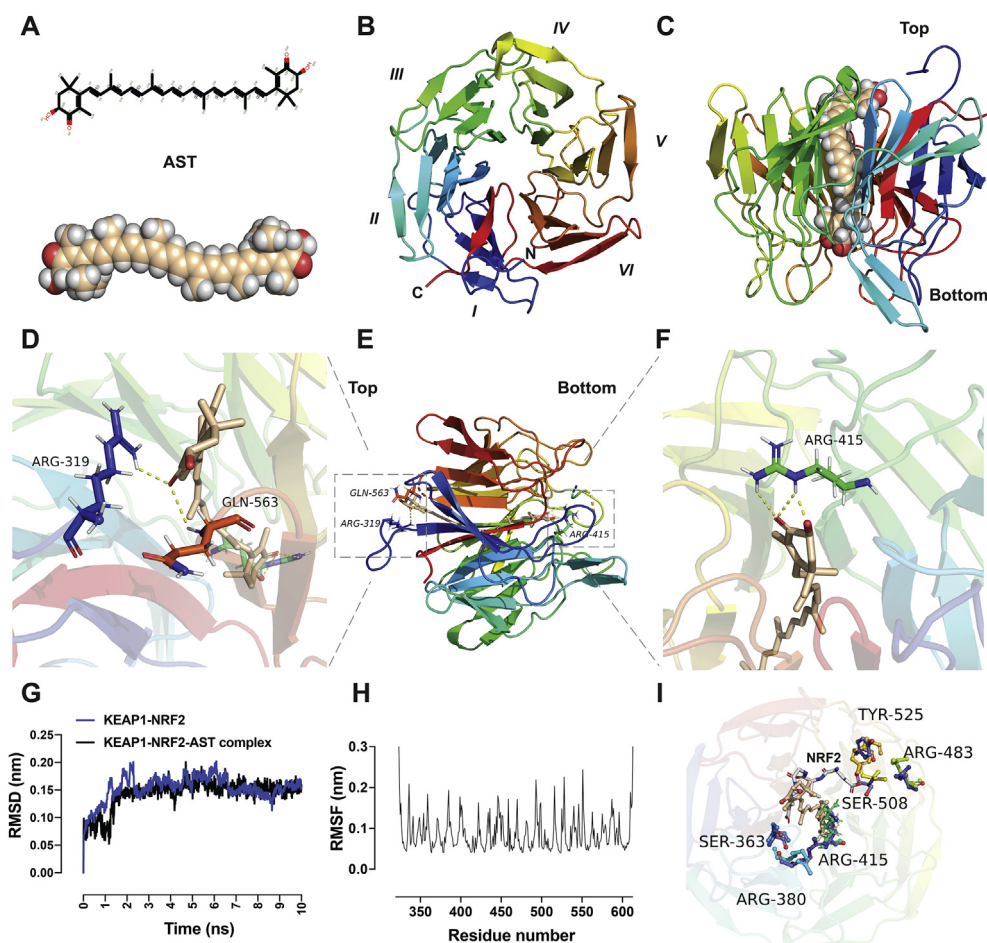
Figure 1 Molecular docking and dynamic analysis of astaxanthine and KEAP1. (A) Molecular structure of astaxanthine. (B) A cartoon representation of the KEAP1−NRF2 (PDB ID: 6LRZ) β-propeller domain is shown from the top view. The propeller domain contains six blades folded into a pseudo-six-fold symmetry. (C) A cartoon representation of KEAP1 in complex with astaxanthine molecule at the center of the protein from the side view. (D)−(F) A cartoon representation of intermolecular interactions between KEAP1−NRF2 and astaxanthine from different views. Astaxanthine exerts hydrophilic interactions with the binding site residues at the top (D) and bottom (F) sites. The important residues establishing the hydrophilic interactions are Arg 319, Arg 415, and Gln 563. (G) RMSD of the KEAP1−NRF2−AST complex and KEAP1−NRF2 obtained within molecular dynamics simulation for 10 ns. (H) The time-averaged RMSF of KEAP1−NRF2 residues was obtained to analyse the local mobility of the protein after docking. (I) Comparison between the KEAP1−NRF2−AST complex and the KEAP1−NRF2 (PDB ID: 5WFV) reveals that astaxanthine partially overlapped with the ETGE motif of the NRF2 peptide. The NRF2-binding sites reveal significant changes in the orientation of residues including Arg 380, Arg415, Arg 483, Ser 508, and Tyr525 after AST docking to KEAP1−NRF2. The figures are generated using *PyMOL*. AST, astaxanthine; PDB, protein data bank; RMSD, root mean square deviation; RMSF, root mean square fluctuations.

USA) and PLIP web server[35] was used for the visualizations and graphics generations. MD simulation of the docked complex was performed in the GROMACS release 2019.4 packages with GROMOS96 54A7 force field. The PRODRG2 server was used to generate the topology of the ligand. The protein−ligand system was embedded in a cubic box of the appropriate size with periodic boundary conditions and a simple point charge water solvation model. The overall system was neutralized by adding 8 K^+ ions to the solution. The SHAKE algorithm was used to constrain all bond lengths involving hydrogen atoms. The long-range electrostatic interactions were treated with the Particle Mesh Ewald method within a cut-off of 12 Å. The overall system was suitably minimized, followed by the NPT and NVT ensemble equilibration steps. The temperature and pressure of 300 K and 1 atm, respectively, were applied. The final production run was carried out with a Parrinello−Rahman barostat to maintain a constant temperature and pressure during the simulation time. A 2 fs time step was applied. The MD simulation of the protein−ligand complex was conducted for 10 ns.

2.2. Mouse models

FVB breeding mice were purchased from the Department of Laboratory Animal Science of Fudan University (Shanghai, China) and used for the cisplatin treatment experiments. Animals were operated under general anesthesia with 100 mg/kg ketamine and 10 mg/kg xylazine sodium intraperitoneal injection. The adequacy of anesthesia was determined by toe pinch. Heating pads were used to maintain the body temperature of animals after complete anesthesia throughout the experimental procedures until they awoke.

2.3. Cell lines

The HEI-OC1 cell line was maintained in high-glucose Dulbecco's modified Eagle's medium (Gibco BRL, Gaithersburg, USA) with 10% fetal bovine serum (Gibco BRL, NY, USA) without antibiotics. These cells were seeded in six-well plates and proliferated under permissive conditions at 33 °C and 10% CO_2 and passaged using 0.25% trypsin/EDTA (Life Technologies, Carlsbad, CA, USA). AST (Cayman Chemical, Ann Arbor, MI, USA) was dissolved at a stock concentration of 8.3 mg/mL in 99% dimethyl sulfoxide (Sigma−Aldrich) and prepared in a culture medium to a final concentration of 10−100 μmol/L. The HEI-OC1 cells were pretreated with AST for 24 h before the addition of 10 μmol/L cisplatin into the culture media and further incubated for 24 h (Fig. 1A and B).

2.4. Cell viability assay

Cell Counting Kit-8 (CCK-8; Sigma−Aldrich) was used to assess cell viability according to the manufacturer's instructions. Briefly, cells were seeded in triplicate at a density of 5000 cells/well in a 96-well plate and incubated overnight under growth conditions. After drug treatment, 100 μL fresh culture medium containing 10% CCK-8 was added to each well for 4 h. Finally, the optical density (OD) values were determined at 450 nm using a microplate reader (Bio-Rad, Hercules, CA, USA). The blank was subjected to the same procedure without cell seeding, while the control was left drug-free. The relative viability was calculated as Eq. (1):

$$Relative\ viability(\%) = \left(A_{experiment} - A_{blank}\right) / \left(A_{control} - A_{blank}\right) \times 100 \tag{1}$$

where A represents absorbance.

2.5. Cochlear explants

Postnatal 3-day (P3) C57BL/6 mouse cochleae were quickly dissected in cold phosphate buffer saline (PBS) and maintained in the culture in four-well plates with culture medium Dulbecco's modified Eagle's medium containing 1% N-2/2% B-27 supplement (Invitrogen, Carlsbad, CA, USA) and 50 IU/mL penicillin (Sigma−Aldrich). After cochlear explants were cultured for 1 day, a culture medium with or without AST was applied for preincubation at 37 °C in 5% CO_2 for 24 h, followed by coincubation with 50 μmol/L cisplatin (Nuoxin; Hansoh Pharmaceutical Co., Ltd., Lianyungang, China). Cisplatin at a concentration of 50 μmol/L was chosen based on the dose−response (10−80 μmol/L), while the explant assay consistently showed that ~50% HCs in the mouse cochleae died at this concentration after ~24 h (Fig. 1D and E). AST at a concentration of 120 μmol/L was chosen based on the dose responses (20−140 μmol/L), while the explant assay consistently showed that ~90% HCs in the mouse cochleae remained at this concentration after 24 h cisplatin exposure (Fig. 1F). The cochleae were fixed with 4% paraformaldehyde and stained with myosin VIIA 488 and DAPI (Sigma−Aldrich) to determine the viability of the HCs. Cochleae were imaged by laser scanning confocal microscopy, at least one 200-μm region from different turns were photographed. The numbers of intact HCs were manually counted in ImageJ. For each experimental condition, a minimum of three independent cochleae were collected and tested.

2.6. Detection of ROS production

Fluorescent probe 2,7-dichlorofluorescein diacetate (DCFH-DA; Beyotime, Shanghai, China) was used to evaluate the intracellular ROS production. The samples from different treatments were washed in PBS and then incubated with 10 μmol/L DCFH-DA in serum-free medium at 37 °C for 30 min in the dark. Nuclei were labelled with DAPI at 37 °C for 10 min and quantification of the mean fluorescence intensity (488 nm excitation/525 nm emission) was performed with a Leica SP8 confocal fluorescence microscope under the same settings. The positive control was treated by the ROSup (the ROS Assay Kit) used as the stimulator that can definitely increase cellular ROS level. Cells were also analysed using flow cytometer (MoFlo XDP; Life Sciences, Fort Collins, CO, USA) with an excitation wavelength of 488 nm to evaluate the intracellular free radical level after centrifugation and re-suspension.

2.7. Mitochondrial membrane potential (MMP) evaluation

The fluorescent dye MitoTracker Red CMXRos (MTRC; Beyotime) was used for monitoring MMP. Cochlear explants and HEI-OC1 cells from different treatments were washed in PBS and then incubated with 200 nmol/L MTRC in a medium at 37 °C for 30 min in the dark. Nuclei were labeled with DAPI for 10 min at 37 °C and quantification of the fluorescence intensity (579 nm excitation/599 nm emission) was performed with a Leica SP8 confocal fluorescence microscope under the same settings.

2.8. Cellular apoptotic markers assay

Immunofluorescence was employed to localize DNA damage response proteins and apoptotic markers in cultured cochlear explants using monoclonal rabbit antibody against cleaved caspase-3 (Cell Signaling Technology, Danvers, VA, USA), monoclonal mouse antibody against myosin VIIA, and monoclonal rabbit antibody against myosin VIIA (Proteus Biosciences, Ramona, CA, USA). Primary antibodies were decanted in PBS and the samples were incubated for 1 h at 37 °C with the secondary antibody donkey anti-rabbit 488 (1:500 dilution, Invitrogen) and donkey anti-mouse 555 (1:500 dilution, Invitrogen) to label hair cells. The cell nuclei were counterstained with DAPI. Annexin V conjugated to FITC kit (Beyotime) was used to detect the cell surface localization of phosphatidylserine according to the manufacturer's instructions. For the TUNEL (terminal deoxynucleotidyl transferase-mediated dUTP nick-end labelling) test, the cochleae were rinsed with PBS three times for 10 min each and then treated with the in situ cell death detection kit (Beyotime) according to the manufacturer's instructions. All fluorescence images were obtained using a Leica TCS SP8 confocal laser-scanning microscope. All images were processed and analysed using the ImageJ software.

2.9. RNA isolation and quantitative PCR

Eight cochlear explants from each experimental group were pooled for RNA extraction due to the extremely minute samples that were extracted from the cochlear explants. Cochlear explants were washed twice with PBS after incubation, and total RNA was extracted using TRIzol reagent (Invitrogen) following the manufacturer's instructions. All tissues contributing to the pooled sample underwent the same treatment conditions. The quantity

and quality of isolated RNA were analyzed with a NanoDrop 2000 spectrophotometer (Thermo Fisher Scientific, Waltham, MA, USA), and the OD 260/280-nm absorbance ratios for all samples were between 1.8 and 2.1. Total RNA was reverse transcribed into cDNA using Superscript III reverse transcriptase (Invitrogen). Quantitative PCR (qPCR) was performed with an ABI 7500 Real-Time PCR system (Applied Biosystems, USA) and the TB Green PrimeScript RT-PCR Kit (Takara, Shiga, Japan). All primers used in this study are listed in Supporting Information Table S1. Actin, a housekeeping gene, was used for endogenous control. Each PCR reaction was carried out in triplicate, and the relative gene expression was quantified using the $2^{-\Delta\Delta Ct}$ method.

2.10. Western blotting assay

The RIPA lysis buffer (Biomiga, San Diego, CA, USA) was used for whole lysates of HEI-OC1 cell preparation after adding a protease inhibitor cocktail (Sigma−Aldrich). The lysates were centrifuged at $12,000 \times g$ for 10 min at 4 °C, and the supernatants were collected for protein analysis. Protein concentrations in protein solutions were determined using the BCA protein assay kit (Beyotime). Equal amounts of each cell lysate were loaded onto 15% SDS-PAGE and transferred onto polyvinylidene difluoride membranes (Millipore, Schaffhausen, Switzerland). The following antibodies were used for immunoblot analysis: anti-active caspase-3 rabbit (A11021), anti-BAX rabbit (A19684), anti-BCL-2 rabbit (A0208), anti-NRF2 rabbit (A1244), anti-HMOX1 rabbit (A1346), anti-NQO1 rabbit (A19586), and anti-β-actin rabbit (AC038) obtained from ABclonal Technology (Woburn, MA, USA). The antibodies were used at dilutions ranging from 1:500 to 1:1000. Subsequently, the membranes were washed in TBST three times for each 10 min and then incubated with HRP-conjugated secondary antibody (1:5000 dilution) at 37 °C for 1 h. The protein bands were scanned and displayed using the SuperSignal West Dura chemiluminescent substrate kit (Thermo Fisher Scientific). ImageJ software was used to quantify the band intensities relative to the loading control β-actin expression. Each Western blot series (n) was carried out using cell lysates from three replicated samples.

2.11. Cisplatin-induced hearing loss mouse

A 4 mg/mL stock solution of cisplatin was prepared in sterile saline (0.9% NaCl) at 37 °C. FVB mice received 2 mL of warm saline *via* intraperitoneal injection one day before 4 mg/kg cisplatin administration *via* intraperitoneal injection. Next, 2 mL of warm saline was injected once per day for two consecutive cisplatin cycles to ameliorate dehydration after cisplatin injection. For intratympanic injection, a stock solution of AST was diluted to 400 µmol/L with 1 mL 30% poloxamer 407 (Sigma−Aldrich) at 4 °C for 24 h. For cisplatin protocols, the mice were given the same treatment of AST (400 µmol/L) *via* intratympanic administration 1 day before each cisplatin cycle. Less than 20% mortality was observed in both cisplatin and combined cisplatin and AST treatments.

2.12. Auditory brainstem response (ABR) threshold

ABR was measured in anesthetized animals one week before drug administration and 14 days after cisplatin treatment. After anesthetization, mice were positioned on a heated pad maintained at 37 °C in a soundproof booth. Three needle electrodes were

compromised by a noninverting electrode placed at the vertex of the midline, inverting electrode placed over the mastoid of the target ear, and the ground electrode placed at the base of the tail. A low-impedance Medusa digital biological amplifier system (RA4L; TDT; 20-dB gain) was used to collect the signals. Following visual inspection of stacked waveforms at each frequency, the stimulus intensity ranged from 90 to 0 dB in 5 dB steps to identify the threshold decibel SPL above the noise floor, at which a visible and repeatable signal wave was recorded in two averaged runs. Averaged ABR waveforms were obtained from responses to 500 tone bursts at each test frequency. The signals collected by the electrodes were amplified 10,000 times with band-pass filters set between 100 and 3 kHz. To facilitate recovery from anesthesia, we tapped lightly at their lower limbs with an index finger. We did not manipulate the animals until they regained voluntary movement.

2.13. Immunofluorescence sample preparation and staining

The cochleae from adult mice were dissected from the temporal bones and fixed in 4% paraformaldehyde at 37 °C for 60 min. After three rinses with PBS, the cochleae were soaked in 10% EDTA for 3-day decalcification. The entire cochlear explant was divided into three equal parts presented as the basal, middle, and apical turn. The primary antibody used in our study was an anti-myosin VIIA antibody (1:500 dilution; Proteus Biosciences). After washing three times with PBS to remove the unbound primary antibodies, the samples were incubated for 1 h at 37 °C with the secondary antibody donkey anti-rabbit 488 (1:500 dilution, Invitrogen). Nuclei were counterstained with DAPI (1:800 dilution, Sigma−Aldrich) at 37 °C for 10 min, and the samples were mounted and imaged under a Leica SP8 laser scanning confocal fluorescence microscope (Leica Microsystems, Biberach, Germany).

2.14. Statistical analysis

Statistical analyses were performed using the GraphPad Prism Software. Data were analysed using the one-way or two-way ANOVAs with Bonferroni correction for the mean difference.

3. Results

3.1. Molecular docking and dynamic simulation between AST and KEAP1−NRF2

Fourteen known small-molecule drugs for protecting against cisplatin ototoxicity were selected, and compared with the docking of AST and KEAP1−NRF2. The formulations of all recruited small molecules are obtained from the Drugbank database (Supporting Information Fig. S1). The KEAP1−NRF2 (PDB ID:6LRZ) protein is obtained from the PDB database. Protein−ligand semi-flexible docking performance is processed between small molecules and KEAP1−NRF2 and evaluated by the final interaction score. All the selected small molecule compounds could dock with KEAP1−NRF2 protein, and AST had the highest binding energy score with KEAP1−NRF2 protein (Supporting Information Table S2). Molecular docking analysis of KEAP1−NRF2−AST complex reveals that AST yields prominent interaction for two binding sites, one oriented at the bottom of the NRF2-binding site and one at the top of the loop (Fig. 1C−F). Hydrogen bonds are exerted on both end rings of AST molecule with residues Arg 319, Arg 415, and Gln 563

(Fig. 1D−F). At the bottom site, hydrogen bonds are observed between the terminal β-ionone ring and the Arg415 residue. Another β-ionone ring interacts directly with the residues Arg319 and Gln563 which are positioned at the top region of KEAP1. To estimate the binding stability of protein−ligand complexes under dynamic conditions, we performed KEAP1−NRF2−AST complex simulation for 10 ns. The root means square deviation (RMSD) of the backbone of KEAP1 was obtained to examine the stability of trajectories for unliganded target KEAP1−NRF2 and target KEAP1−NRF2−AST complex[36]. It was discovered that the RMSD reached equilibrium and fluctuation around the mean value after a 3-ns simulation (Fig. 1G). The stable RMSD value for KEAP1−NRF2−AST complex was lower than that of the original KEAP1−NRF2 protein. The time-averaged root means square fluctuations of protein residues were obtained to analyze the local mobility of proteins[37]. The average value of root means square fluctuations was lower than 0.1 nm and the key amino acids were consistent with the process shown in Fig. 1H. These trajectories indicate that the complex of KEAP1−NRF2−AST maybe have a relatively stable conformation and astaxanthine maybe have a competitive effect on KEAP1−NRF2 peptide targets.

3.2. AST reduces cisplatin-induced ototoxicity in the HEI-OC1 auditory cell line

To identify the optimal cisplatin-induced ototoxicity model *in vitro*, increasingly concentrated cisplatin (0, 5, 10, 15, 20, 30, 40, 50, 60,70, 80, and 90 μmol/L) was applied to the HEI-OC1 cells for 24 h, and cell viability was analyzed by the CCK-8 assay. Compared with the untreated control group, the cell viability of cisplatin treatment was significantly reduced in a dose-dependent manner (Fig. 2A). Cisplatin at a concentration of $IC_{50} = 10$ μmol/L reduced cell viability by 50%. Therefore, a cisplatin concentration of 10 μmol/L was used for the following *in vitro* study. To determine the effects of AST on the HEI-OC1 cells after cisplatin treated, these cells were pretreated with AST at concentrations of 10, 20, 30, 40, 50, 60, 70, 80, 90, and 100 μmol/L for 24 h, and then co-treated with 10 μmol/L cisplatin for 24 h. We found significant protection of AST at 80, 90, and 100 μmol/L, and an optimal protective effect at a concentration of 80 μmol/L compared with cisplatin alone (****$P < 0.0001$, Fig. 2B). These results indicate that AST exerted protection on the viability of HEI-OC1 cells against cisplatin ototoxicity *in vitro*.

3.3. AST protects against cisplatin-induced HC loss in the mouse cochlear explants

Firstly, we identified the spatial and temporal patterns of HC death in the mouse cochleae following cisplatin injury. The P3 C57BL/6 mouse cochlear explants were exposed to cisplatin at increasing concentrations (10, 20, 30, 40, 50, 60, 70, 80, and 100 μmol/L) for different durations (6, 12, 18, 24, 36, and 48 h) (Fig. 2C−E and Supporting Information Fig. S2). It was found that cisplatin resulted in substantial and concentration-dependent HC degradation in the basal turn of the cochlear explants. Survival HC counts following cisplatin exposure at a close concentration of $IC_{50} = 50$ μmol/L show a time-dependent HC loss accompanied by a dramatic fading within 18−24 h in the basal turn (Fig. 2D and E).

Next, we investigated the cytoprotective effects of AST at different concentrations (20, 40, 60, 80, 100, 120, and 140 μmol/L) using P3 C57BL/6 mouse cochlear explants pretreated with AST for 24 h, followed by 50 μmol/L cisplatin treatment for 24 h. The numbers of surviving HCs per 150 μmol/L per treatment were counted manually. Medium-only, drug-only, and cisplatin-only treatments were displayed as controls. The hair cell survival results reveal that the percentages of viable hair cells in the AST pretreatment group (AST + CDDP) treated with various concentrations were 64.5 ± 3.3%, 72.1 ± 8.1%, 63.2 ± 12%, 69.9 ± 4%, 77.8 ± 11.3%, 87.7 ± 5.2%, and 63.4 ± 7.2%, respectively (Fig. 2F). Therefore, quantified data suggest that AST attenuated cisplatin-induced cytotoxicity in cochlear explants. We chose AST at the concentration of 120 μmol/L with the optimal HC protection in the following experiments (Fig. 2G).

To identify the essence of cisplatin-induced HC loss, we preliminarily explored representative apoptotic markers. The staining for cell surface Annexin V and nuclei TUNEL after cisplatin exposure showed two different phases of apoptosis in HCs. Altogether, these results indicate that cisplatin could induce hair cell damage relative to apoptosis (Fig. 2H and I).

3.4. AST inhibits cisplatin-induced ototoxicity involving the activation of the NRF2-mediated pathway

According to the molecular docking and dynamics results, we hypothesized that the increased HC survival in the AST-pretreated group compared with the cisplatin treatment contributed to the activation of NRF2 mediated pathway by AST. To identify the mechanism responsible for AST protection against cisplatin ototoxicity, we investigated the levels of *Nrf2* and downstream genes both in HEI-OC1 cell line and cochlear explants in different treatments. We performed qPCR in three biological replicates to investigate the influence of AST on the expression of *Nrf2*, *Hmox1*, and *Nqo1* in cochlear explants from P3 mice of both sexes. Incubation of cochlear explants with AST pretreatment for 24 h before cisplatin exposure led to a higher accumulation of *Nrf2*, *Hmox1*, and *Nqo1* than that in the cisplatin-only treatment (Fig. 3A). This was consistent with the protein levels in HEI-OC1 cells (Fig. 3B). Notably, cochlear explants treated with 50 μmol/L cisplatin led to a decrease in *Nrf2* and *Nqo1* gene expression levels compared with that in the control (Fig. 3A).

Furthermore, we proved that AST protected against cisplatin ototoxicity *via* activating the *Nrf2* mediated pathway. ML385, a *Nrf2* specific transcriptional activity blocker[27], was applied in the AST-pretreated cochlear explants. It was shown that coincubation of AST and ML385 leads to substantial HC loss following cisplatin treatment (AST/CDDP/ML385) compared with the AST-only pretreatment (AST/CDDP, Fig. 3C and Supporting Information Fig. S3). No toxicity and a significant difference were observed in the ML385-only group (10 μmol/L) compared with the control group in P3 C57BL/6 mouse cochlear explants (Fig. S3). Co-incubation of both AST and ML385 before cisplatin treatment successfully caused a 31% reduction of the *Nrf2* mRNA level in HCs (Fig. 3D). Interestingly, it was also shown that blockage of *Nrf2* partially inhibited downstream genes including *Hmox1* (Fig. 3D).

3.5. AST attenuates cisplatin-induced oxidative damage and mitochondrial dysfunction

We investigated the oxidative status and effects of AST on intracellular ROS expression both in HEI-OC1 cells and HCs in mouse cochlear explants after cisplatin exposure. Following cisplatin treatment, intracellular ROS levels were evaluated using
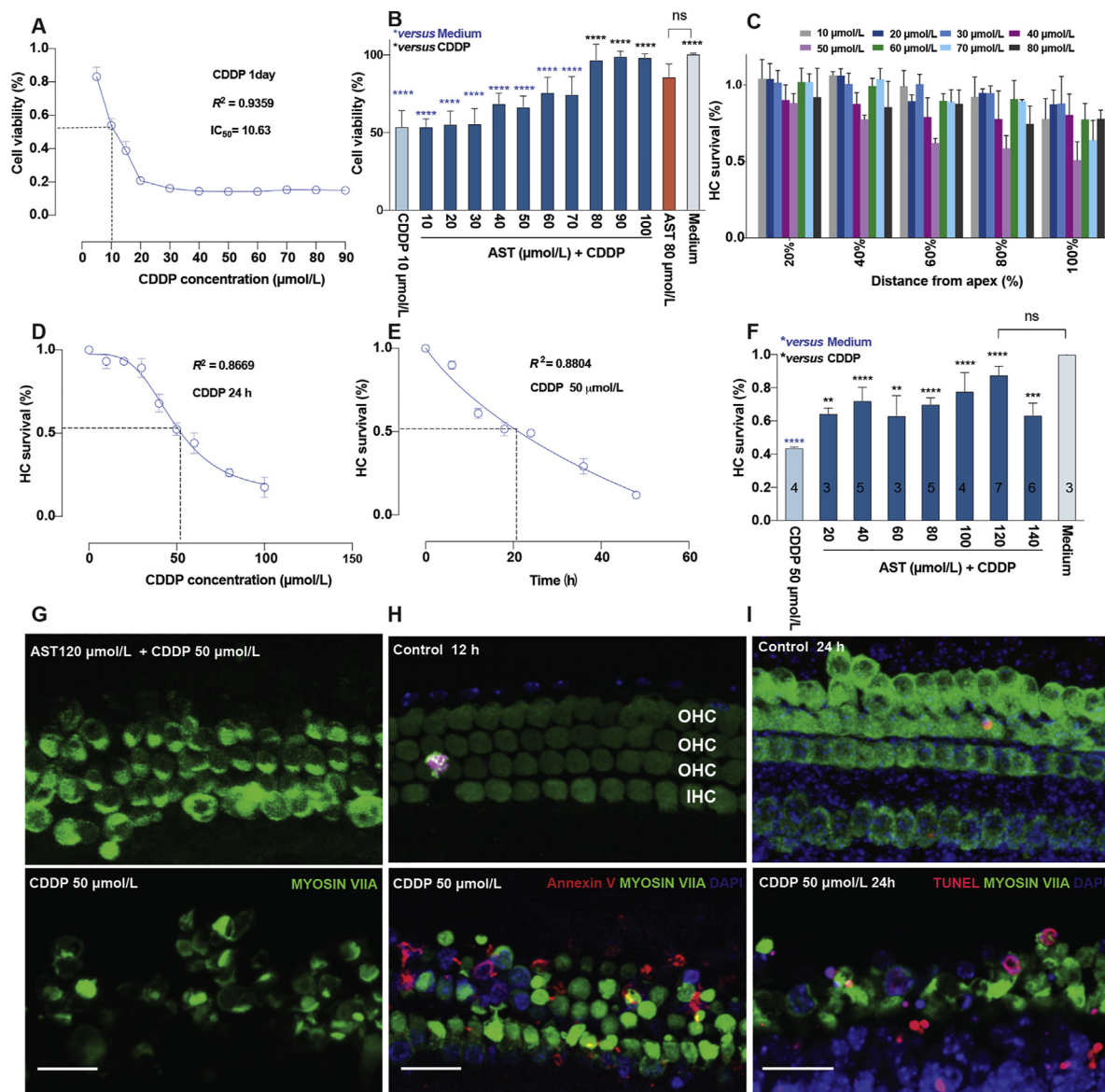
Figure 2 Astaxanthine protection against cisplatin-induced ototoxicity both in cochlear explants and HEI-OC1 cell line modes. (A) A cell pattern for screening in dose−response using HEI-OC1 cell line after 24-h cisplatin exposure. Cisplatin reduced 50% of the cells in the presence of 10 μmol/L that was applied in the following experiments ($n = 4−6$ for cisplatin groups, details shown in data excel). (B) Astaxanthine responsible for dosage protects against 10 μmol/L cisplatin in cell line (dark blue), accompanied by the medium alone (grey), cisplatin alone (light blue), astaxanthine (orange). Cell viability was measured by the CCK-8 kit. Values were presented as the mean ± SD, ****$P < 0.0001$ compared with cisplatin only (black) and medium only (blue) by one-way analysis of variance (ANOVA) with Bonferroni correction ($n = 6$ for medium group; $n = 6$ for AST + CDDP group; $n = 3$ for 80 μmol/L AST group; $n = 5−6$ for cisplatin group; details shown in data excel). (C) Various regions in cochlear explants were treated with different doses of cisplatin for 24 h. Cytotoxicity was evaluated by HC survival in different regions. The distance from the apex is presented as 20%, 40%, 60%, 80% and 100%. Cisplatin dose- (D) and time-dependent (E) curve in the basal turn of cochlear explants. Cisplatin reduces 50% HCs in the presence of 50 μmol/L within 24 h, which was applied in the following experiments ($n = 3−10$ for cisplatin group in D; $n = 7−15$ for cisplatin group in E; details shown in data excel). (F) Dose−response of astaxanthine in postnatal 3-day C57BL/6 mouse cochlear explants damaged with or without cisplatin. Medium only (grey), cisplatin only (light blue), or astaxanthine pretreated for 24 h before cisplatin treatment for 24 h (AST + CDDP, dark blue) in explants. Numbers embedded in each bar represent the number of explants counted per group. HC survival evaluated by the percentage of the remaining numbers of HCs per 150 μm of the basal turn regions that were stained by MYOSIN VIIA, mean ± SD, **$P < 0.01$, ***$P < 0.001$, ****$P < 0.0001$ compared with cisplatin only (black) and medium only (blue) by one-way analysis of variance (ANOVA) with Bonferroni correction. (G) Representative confocal images presenting the protection of astaxanthine (120 μmol/L) against cisplatin (50 μmol/L) injury in the basal turn of the cochlea. (H) and (I) Representative confocal images show cochlear explants treated with either medium only or 50 μmol/L cisplatin for 12 h (G) or 24 h (H) in the basal region. The numbers of HCs were identified using Myosin VIIA staining (green), fluorochrome-labeled Annexin V (red in G), and TUNEL staining (red in H). Scale bar = 20 μm ns, not significant; AST, astaxanthine; CDDP, cisplatin; HC, hair cell; OHC, outer hair cell; IHC, inner hair cell; TUNEL, terminal deoxynucleotidyl transferase-mediated dUTP nick-end labeling.
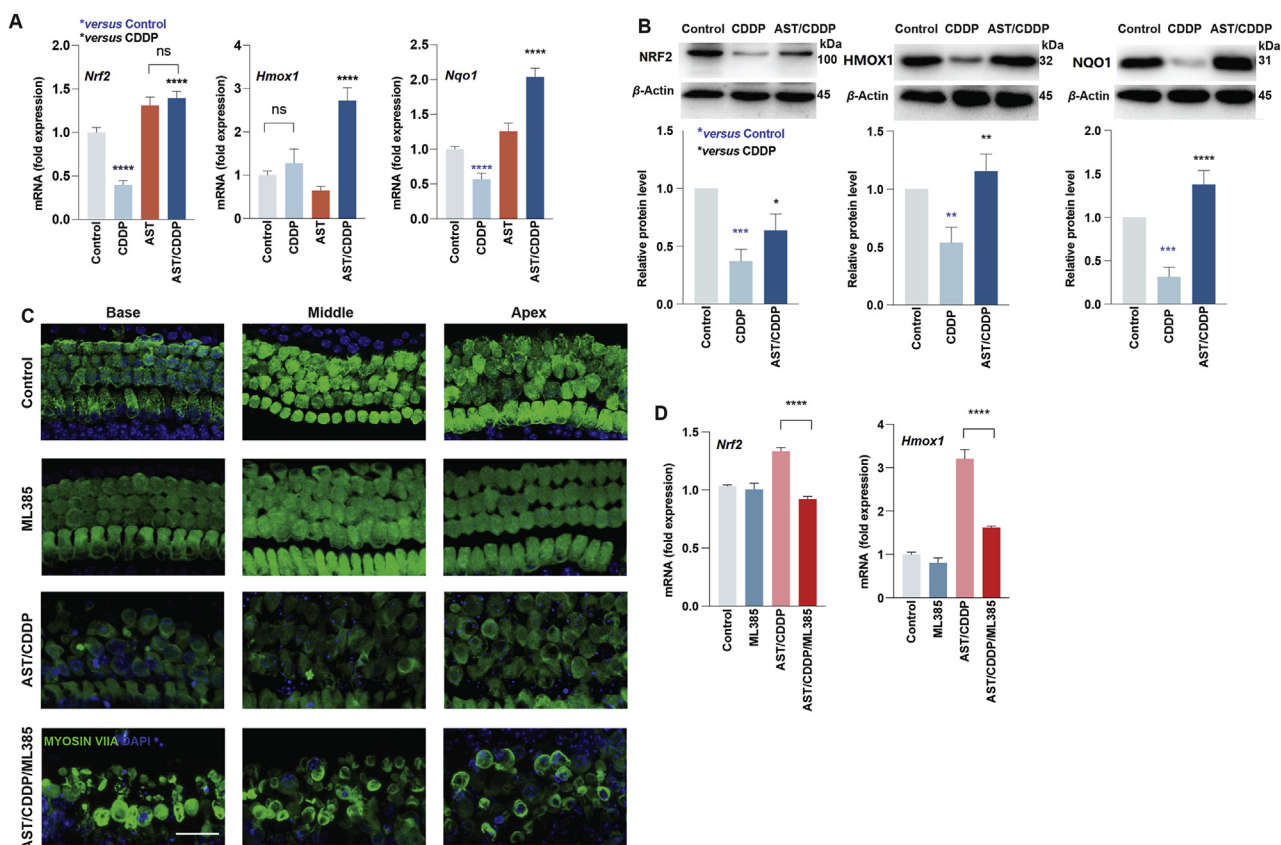
Figure 3 Astaxanthine protects against cisplatin-induced cell death *via* NRF2-mediated pathway. (A) Quantitative analysis of mRNA levels of *Nrf 2*, *Hmox1*, and *Nqo1* in cochlear explants from different treatments. Data are presented as mean ± SD, ****$P < 0.0001$ compared with control (blue) and CDDP (black) by one-way ANOVA with Bonferroni correction ($n = 4-6$ for each group; details shown in data excel). (B) Representative Western blot images of NRF2, HMOX1, and NQO1 in HEI-OC1 cell lines from different treatments. The protein band intensities relative to the loading control β-actin expression were measured by ImageJ software. Data are presented as mean ± SD, *$P < 0.05$, **$P < 0.01$, ***$P < 0.001$, ****$P < 0.0001$ compared with control (blue) and CDDP (black) by one-way ANOVA with Bonferroni correction, $n = 3$ for each group. (C) Representative Myosin VIIA (green) and DAPI (blue) stained confocal images of postnatal 3-day C57BL/6 mouse cochlear explants from the control, ML385, AST/CDDP, and AST/CDDP plus ML385 (AST/CDDP/ML385) groups. Scale bars = 20 μm. (D) Quantitative analysis of mRNA levels of *Nrf2* and *Hmox1* in cochlear explants from different treatments. Data are presented as mean ± SD, ****$P < 0.0001$ compared with the AST/CDDP/ML385 group by one-way ANOVA with Bonferroni correction ($n = 3-4$ for each group; details shown in data excel). ns, not significant; AST, astaxanthine; CDDP, cisplatin; Base, basal turn; Middle, middle turn; Apex, apical turn.

the DCFH-DA assay which is a popular probe for evaluating intracellular hydrogen peroxide. Our results show that the mean fluorescence intensity of DCFH-DA staining significantly increased following cisplatin damage compared with the medium-only controls. This indicates a remarkable amount of ROS production within these HEI-OC1 cells (Fig. 4A). In contrast, the mean fluorescence intensity of DCFH-DA staining was significantly reduced in AST-pretreated cells compared with cisplatin treatment (Fig. 4A). Both flow cytometry and staining results show that the ROS levels increased with cisplatin exposure compared with the medium-only treatment (Fig. 4A and B). Pretreatment with AST significantly decreased the ROS levels in HEI-OC1 cells compared with the cisplatin treatment (Fig. 4C). The same results were observed in the middle regions of P3 mouse cochlear explants without fixation (Fig. 4D and E). These results suggest that AST significantly decreased the over-expression of ROS after cisplatin injury both in HEI-OC1 cells and HCs.

Moreover, to explore the role of mitochondria in cells treated with cisplatin, we detected the MMP using MTRC both in HEI-

OC1 cell line and mouse cochlear explants. As shown in Fig. 5A, cisplatin treatment led to significant loss of MMP in HEI-OC1 cells, which was reflected by the decrease in red fluorescence compared with the undamaged controls. Pretreatment with AST significantly improved the MMP in HEI-OC1 cells, which was reflected by the increase in red fluorescence compared with cisplatin damage (Fig. 5A and B). Differences in functional mitochondrial densities were determined by examining relative differences in MTRC fluorescence intensity in the middle region of the inner HCs (IHCs) from P3 C57BL/6 mice (Fig. 5C). The MMP in IHCs was significantly lower after CDDP exposure, while IHCs pretreated with AST had significantly greater MTRC intensity compared with the cisplatin treatment (Fig. 5D). These results suggest that AST prevented cisplatin-induced mitochondrial dysfunction in HEI-OC1 cells and HCs.

3.6. AST attenuates cisplatin-induced apoptosis

Based on previous qualitative studies of apoptosis induced by cisplatin, we next used cleaved caspase-3 and TUNEL staining to
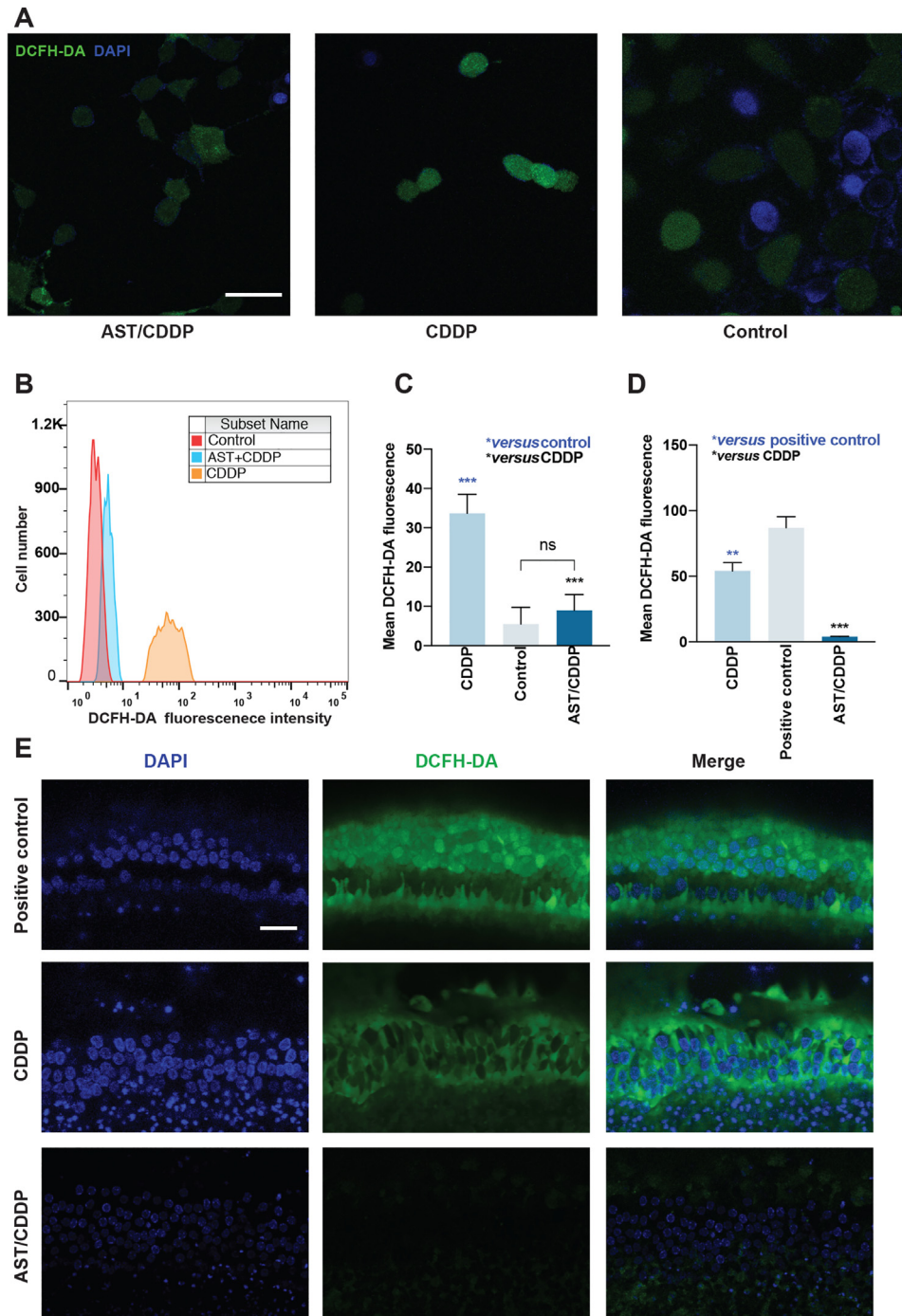
Figure 4 Effects of astaxanthine on ameliorating ROS production in HEI-OC1 cell line and cochlear hair cells. (A)−(C) Representative DCFH-DA (green) and DAPI (blue) stained confocal images of live HEI-OC1 cells from different treatment groups (A). Flow cytometry was used for the analysis of quantitative changes in the mean DCFH-DA fluorescence intensity (B) and (C). The data are presented as mean $\pm$ SD, ***$P < 0.001$, compared with control (blue) and CDDP (black) by one-way ANOVA with Bonferroni correction, $n = 3$ for each group in (C). Scale bar $= 20 \, \mu m$. (D) and (E) Representative DCFH-DA (green) and DAPI (blue) stained confocal images of postnatal 3-day C57BL/6 mouse middle region of live cochlear explants from the positive control, CDDP, and AST/CDDP groups. The ImageJ was used for the analysis of quantitative changes in the mean DCFH-DA fluorescence intensity. The data are presented as mean $\pm$ SD, **$P < 0.01$, ***$P < 0.001$ compared with positive control (blue) and CDDP (black) by one-way ANOVA with Bonferroni correction, $n = 3$ for each group in (D). Scale bar $= 20 \, \mu m$. The positive control was treated by the ROSup (the ROS Assay Kit) used as the stimulator that can definitely increase cellular ROS level. ns, not significant; AST, astaxanthine; CDDP, cisplatin, DCFH-DA, fluorescent probe 2,7-dichlorofluorescein diacetate.
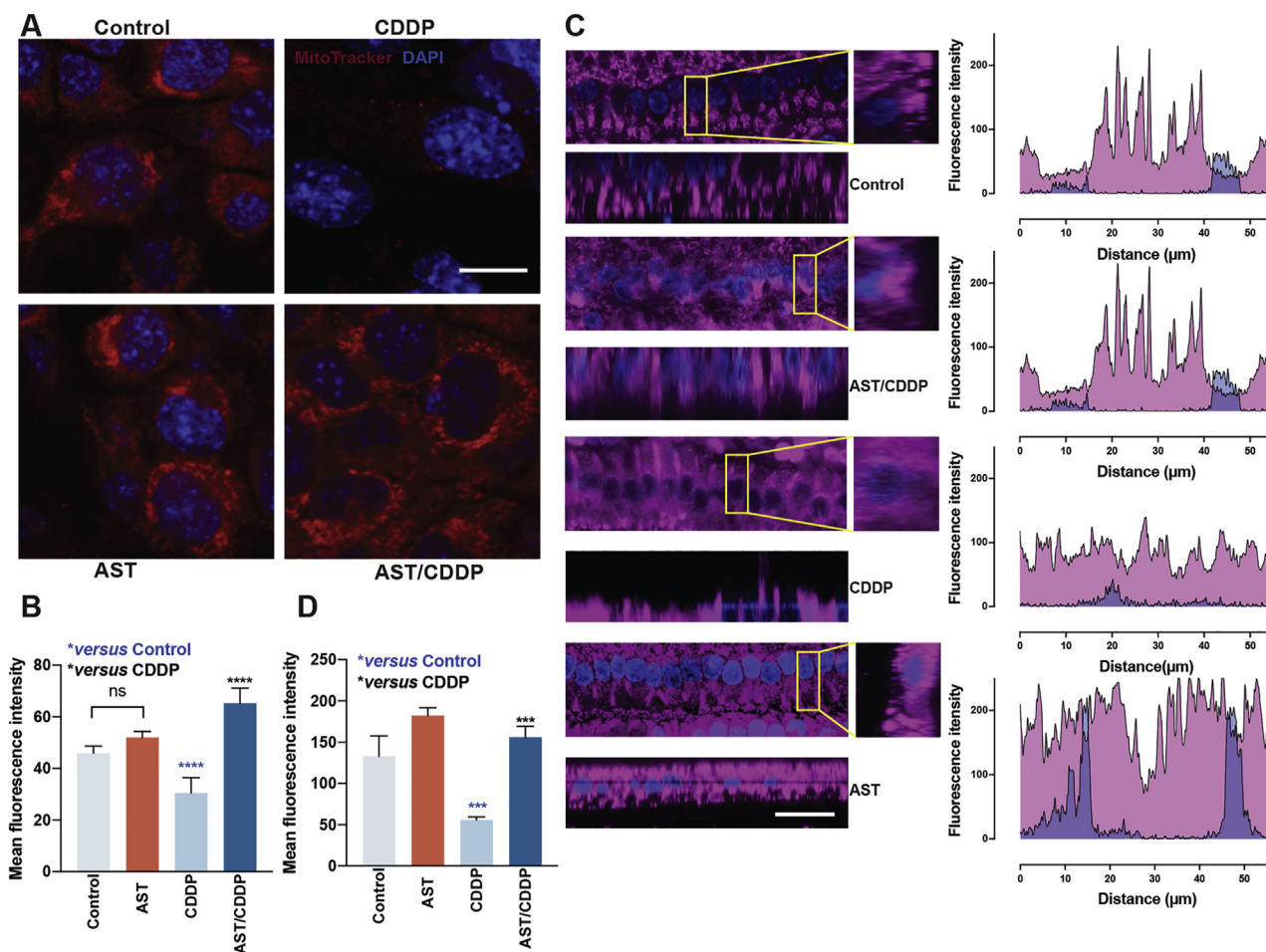
Figure 5 Effects of astaxanthine on maintaining mitochondrial function in HEI-OC1 cell line and IHCs. (A) and (B) Representative MTRC (red) and DAPI (blue) stained confocal images of HEI-OC1 cells from the control, CDDP, AST, and AST/CDDP groups. The ImageJ was used for the analysis of quantitative changes in the mean MTRC fluorescence intensity. The data are presented as mean $\pm$ SD, ****$P < 0.0001$ compared with control (blue) and CDDP (black) by one-way ANOVA with Bonferroni correction, $n = 6$ for each group in (B). Scale bar $= 10$ μm. (C) and (D) Representative MTRC (magenta) and DAPI (blue) stained confocal images of IHCs in middle regions of postnatal 3-day C57BL/6 mouse cochleae from different treatment groups. The Ortho section shows mitochondrial staining of IHCs and the ROI fluorescence from a single IHC in each group was identified under the same microscope settings (C). The ImageJ was used for the analysis of quantitative changes in the mean MTRC fluorescence intensity (D). The data are presented as mean $\pm$ SD, ***$P < 0.001$ compared with control (blue) and CDDP (black) by one-way ANOVA with Bonferroni correction, $n = 3$ for each group in (D). Scale bar $= 20$ μm. ns, not significant; AST, astaxanthine; CDDP, cisplatin; IHC, inner hair cell; MTRC, MitoTracker Red CMXRos; ROI, region of interest.

quantitatively detect the apoptosis induced by cisplatin and inhibited by AST in mouse cochlear explants. Cochlear explants were collected from P3 C57BL/6 mice of both sexes. Cleaved caspase-3 and TUNEL were assayed with cleaved caspase antibody and TUNEL kit in cochlear explants exposed to 50 μmol/L cisplatin for 24 h with or without 120 μmol/L AST pretreated for 24 h. These cochlear explants were then fixed and co-stained with myosin VIIA to identify HCs. The number of cleaved caspase-3-myosin VIIA and TUNEL-myosin VIIA co-staining significantly increased after exposure to cisplatin compared with the medium-only controls (Fig. 6A–D). No cleaved caspase-3 or TUNEL were observed in the medium-only controls. The intensity of cleaved caspase-3 and TUNEL signal in AST-only samples was extremely low. Quantification of the fluorescent signal in Fig. 6B and D

shows a significant difference in signal intensity of various regions between cisplatin-only (CDDP) and AST-pretreated explants (AST/CDDP). AST almost completely inhibited both cleaved caspase-3 and TUNEL staining induced by cisplatin in this assay. It disclosed similar signal intensity levels in AST-pretreated explants compared with those seen in control explants.

Quantitative analysis of qPCR within extrinsic and intrinsic apoptotic genes (caspase-8, *Fadd*, *Bax*, caspase-9, and caspase-3) confirmed the anti-apoptotic activity of AST. Cisplatin significantly increased pro-apoptotic markers including caspase-8, *Fadd*, *Bax*, caspase-3, and caspase-9 (Fig. 6E), while these genes decreased in the AST pretreated groups. The anti-apoptosis ability of AST was also proved by significant decreased protein levels of cleaved caspase-3 and *Bax* in AST-pretreated compared with
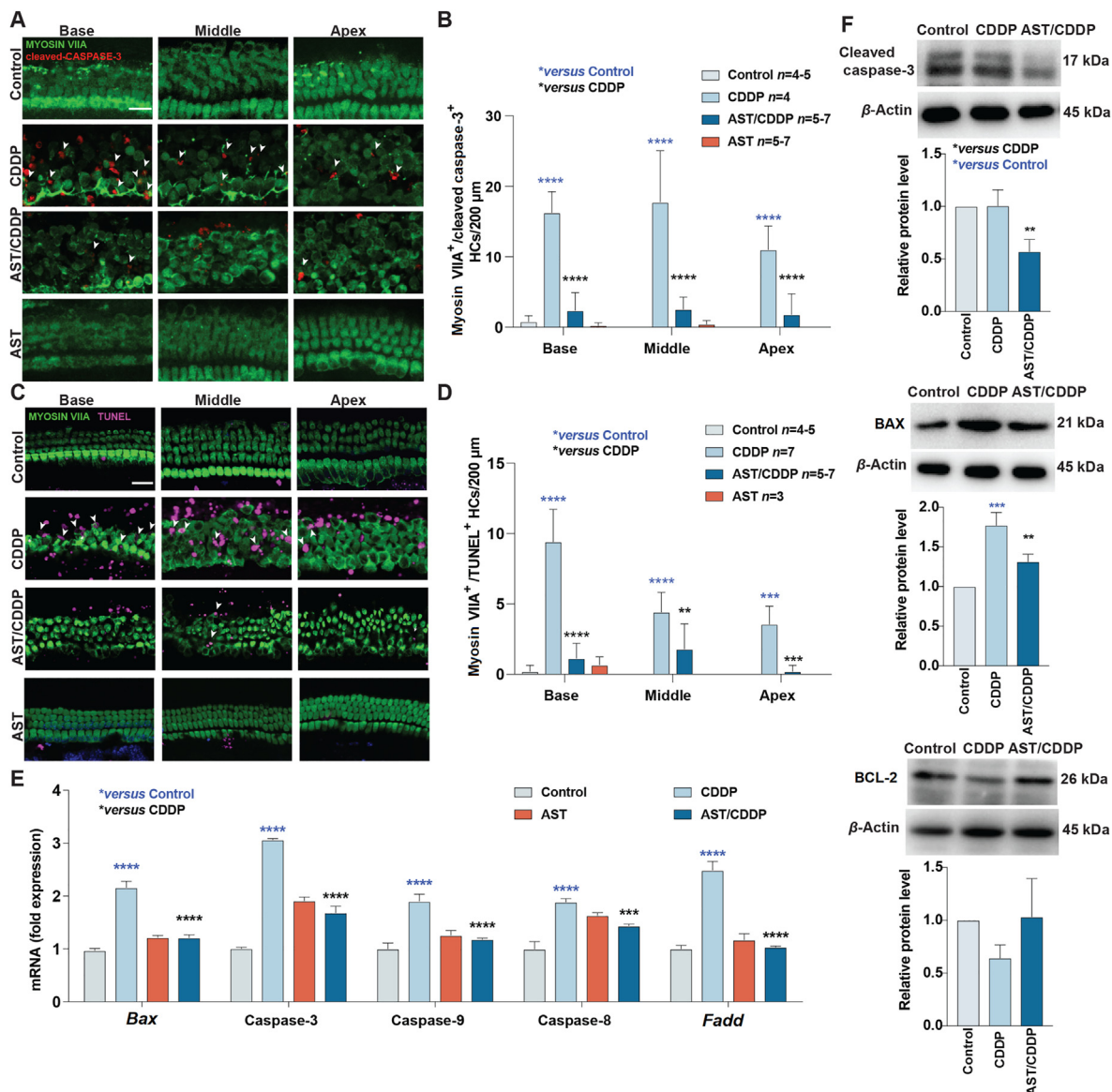
Figure 6 Effects of astaxanthine on cisplatin-induced apoptosis in HEI-OC1 cell line and cochlear hair cells. (A) Representative Myosin VIIA (green) and cleaved caspase-3 (red) stained confocal images of postnatal 3-day C57BL/6 mouse cochlear explants from the control, CDDP, AST, and AST plus cisplatin (AST/CDDP) groups. The co-staining of Myosin VIIA and cleaved caspase-3 are identified with the white labels. Scale bars = 20 μm. (B) Quantification of the numbers of cleaved caspase-3 and Myosin VIIA co-staining cells per 200 μm in the cochlea after the different treatments. The data is presented as means ± SD, ****$P < 0.0001$ compared with control (blue) and AST/CDDP (black) by two-way analysis of variance (ANOVA) with Bonferroni correction. (C) Representative Myosin VIIA (green) and TUNEL (magenta) stained confocal images of postnatal 3-day C57BL/6 mouse cochlear explants from the control, CDDP, AST, and AST/CDDP groups. The co-staining of Myosin VIIA and TUNEL are identified with white labels. Scale bars = 20 μm. (D) Quantitative analysis of the numbers of Myosin VIIA and TUNEL co-staining cells per 200 μm in the cochleae after the different treatments. The data is presented as means ± SD, **$P < 0.01$, ***$P < 0.001$, ****$P < 0.0001$ compared with control (blue) and AST/CDDP (black) by two-way ANOVA with Bonferroni correction. (E) The mRNA expression profiles of apoptotic markers including *Bax*, caspase-3, caspase-8, caspase-9, and *Fadd* in HEI-OC1 cells following different treatments. The values of qPCR were normalized to β-actin and averaged, mean ± SD, ***$P < 0.001$, ****$P < 0.0001$ compared with control (blue) and CDDP (black) by the one-way ANOVA with Bonferroni correction, $n = 3$ for each group. (F) Representative Western blot images of BAX, BCL-2 and cleaved caspase-3 in HEI-OC1 cells from different treatments. All bands of protein were normalized to β-actin and averaged, mean ± SD, **$P < 0.01$, ***$P < 0.001$ compared with control (blue) and CDDP (black) by one-way ANOVA with Bonferroni correction, $n = 3$ for each group. AST, astaxanthine; CDDP, cisplatin; Base, basal turn; Middle, middle turn; Apex, apical turn.

cisplatin treatment in HEI-OC1 cells (Fig. 6F). *Bcl-2*, as an apoptosis suppressor gene, increased in the AST-pretreated compared with cisplatin treatment in HEI-OC1 cells (Fig. 6F). These results indicate that AST inhibited cisplatin-induced apoptosis both in HEI-OC1 cells and mouse cochlear explants.

3.7. Evaluation of AST protection against CIHL

AST exhibited superior antioxidant potency and protective ability against cisplatin-induced ototoxicity both in HEI-OC1 cells and mouse cochleae. Next, we tested the drug potency in adult mice by
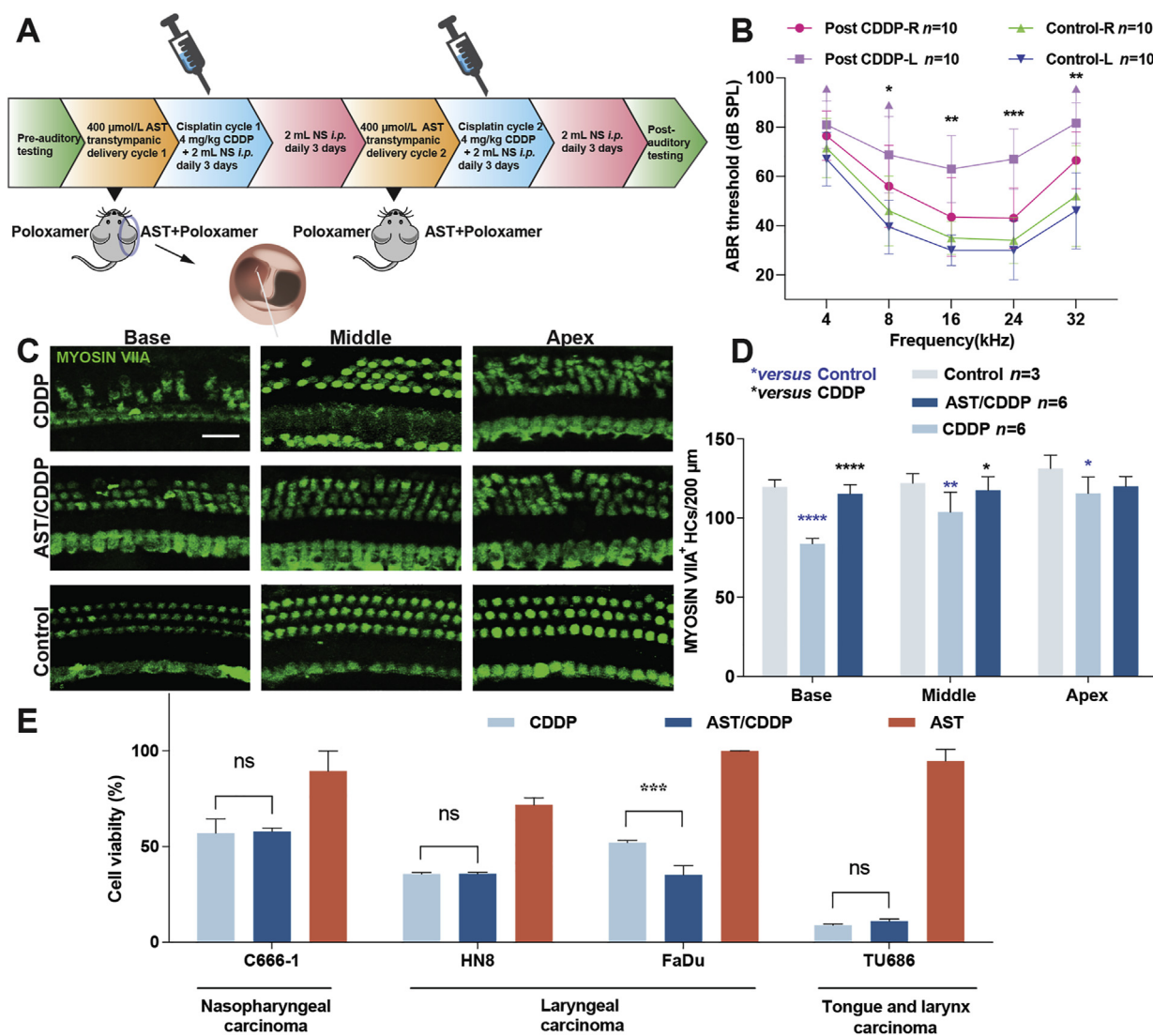
Figure 7 Astaxanthine protects against cisplatin-induced hearing loss in adult mice and does not compromise cisplatin anti-cancer efficacy. (A) Protocol of administration of astaxanthine and cisplatin into postnatal 45-day FVB mice. (B) ABR threshold shifts following protocol from (A). Both left and right ears from the control groups belong to the same mouse. Left and right ears from the same cisplatin-treated mice delivered with the carrier-only (30% poloxamer) and astaxanthine, respectively. Data are shown as mean ± SD, *$P < 0.05$, **$P < 0.01$, ***$P < 0.001$ by two-way ANOVA with Bonferroni correction, $n = 10$ for each group. (C) and (D) Representative Myosin VIIA (green) stained confocal images of postnatal 45-day FVB mouse cochlear explants from the control, CDDP, and AST/CDDP groups. The numbers of HCs per 200 μm in various cochlear regions were counted by Myosin VIIA staining. Data are shown as mean ± SD, *$P < 0.05$, **$P < 0.01$, ****$P < 0.0001$ compared with control (blue) and CDDP (black) by two-way ANOVA with Bonferroni correction. Scale bar = 20 μm. (E) Cell survival of multiple head and neck carcinoma cell lines treated with combination of astaxanthine and cisplatin for 48 h. Purple arrow in B indicates no ABR response at the highest stimulus level tested (90 dB). Data are presented as mean ± SD, *$P < 0.05$, ***$P < 0.001$ compared with cisplatin only by one-way ANOVA with Bonferroni correction ($n = 3$ for each group). ns, not significant; AST, astaxanthine; CDDP, cisplatin; Base, basal turn; Middle, middle turn; Apex, apical turn; NS, normal saline; i.p., intraperitoneal injection.

local trans-tympanic delivery. The protocol specified two rounds of daily treatment with 4 mg/kg cisplatin for 3 days followed by 3-day recovery (Fig. 7A). Trans-tympanic administration was used for AST delivery 1 day before the cisplatin cycle, as this method is practicable and manageable in clinics and the general population[38]. As described in Fig. 7A, the baseline ABR thresholds for P45 FVB mice were established 7 days before experimental procedures, and both ears showed no significant difference (Fig. 7B). Mice treated with the carrier (30% poloxamer) only showed no significant threshold shift (not shown). The left ears injected with carrier alone in cisplatin-treated mice had significantly raised

threshold shifts at frequencies of 16, 24, and 32 kHz. The contralateral right ears pre-treated with AST in cisplatin-treated mice had significantly decreased threshold shifts, with an average reduction of 20 dB at 16 and 24 kHz, and 15 dB at 32 kHz. Morphological analysis of cochlear hair cell counting revealed significant HC loss in cisplatin-only treated animals compared with that in the controls. The greatest hair loss was found in the basal region, which corresponded to ABR threshold shifts (Fig. 7C and D). Hair cell loss was limited in the right ears pre-treated with AST in cisplatin treated mouse modes, which disclosed the protective efficacy of the drug. No hair cell loss was

observed in mice treated with AST (not shown). Hence, the combination of acoustic tests and morphological HC counting strongly indicate that local delivery of AST can prevent HC loss in mouse cochleae and exert protective effects against CIHL in adult mice.

3.8. AST does not interfere with cisplatin killing efficacy in tumor cell lines

Currently, there is no consensus on the advice of taking antioxidant agents during cisplatin chemotherapy. However, accumulative evidences from different studies showed that antioxidant supplements may reduce the side effects from chemotherapy[39]. Although AST is proved to protect against cisplatin ototoxicity in multiple models, it is also necessary to confirm whether the drug hinders the cisplatin potential in chemotherapy before it can be allowed for clinical application. Hence, four human head and neck cancer cell lines C666-1, HN8, Fadu and TU686 were used to testify AST effects on cisplatin killing ability in tumor cells. Cancer cells were treated with the combination of AST and cisplatin for 48 h, and then the viability was measured by CCK-8 assay. Medium-only, cisplatin-only, and AST-only treated cells were set as controls, and the viability was presented as percentage compared with medium only (Fig. 7E). AST was identified to have no inhibition on cisplatin-induced tumor cell death. Altogether, these data indicated that AST had no interference with cisplatin efficacy in killing tumor cells.

4. Discussion

Cisplatin is a widely used chemotherapeutic agent for patients with cancer and has a high degree of ototoxicity (average incidence > 60%)[40−42]. However, only a few of them have been shown to confer any protection on clinical patients, and none of them is FDA-approved. Thus, an urgent unmet medical need for screening drugs that can be administered to patients during chemotherapy to prevent and protect hearing loss. Our study is to report that the novel superior antioxidant drug AST protects against cisplatin-induced ototoxicity by activating the NRF2 mediated pathway without interfering with cisplatin chemotherapeutic efficacy in tumor cells.

The expression of a wide array of antioxidant genes were regulated by NRF2 that is proved to have important roles in the cellular protection system, especially in oxidative stress mediation[43−46]. Here, we hypothesized that AST directly interacted with KEAP1, a predominant repressor of NRF2. The blockage of the KEAP1−NRF2 interaction is known to be a potential target for the development of drugs against neurodegenerative diseases[47]. In our study, the molecular docking and dynamic analysis of KEAP1−NRF2−AST complex were performed and it revealed that AST molecule can exactly bind to the active pocket of KEAP1. The residues located at the binding sites after dynamic simulation were altered compared with the original protein crystal structure. Superposition of the docking complex on the NRF2 peptide complex (PDB ID: 5WFV) reveals that the residues at the NRF2-binding sites in the KEAP1 crystal structure did not significantly change the orientation except Arg415, Arg483, Ser508, and Tyr525 (Fig. 1G). In addition, we found that the binding regions (Gly81−Glu82 residues) where the AST molecule was docked to KEAP1 partially overlapped with the ETGE motif where NRF2 binding to KEAP1. Thus, our results suggest that AST might exert a competitive inhibition of NRF2 binding to the Kelch domain of KEAP1 via binding to residue Arg415 for hydrogen connection. This mechanism is similar to that dimethyl fumarate competes with NRF2 to bind to the Kelch domain of KEAP1[48].

As anticipated, we found that AST protected against cisplatin-induced ototoxicity via NRF2 mediated pathway both in HEI-OC1 cell line and mouse cochlear explants. We found that AST resulted in significant increased mRNA and protein levels of Nrf2, Hmox1, and Nqo1 in AST/CDDP group compared with CDDP group, while these levels were decreased in CDDP group compared with the control (Fig. 3C and D). Furthermore, the inhibition of NRF2 in the AST/CDDP/ML385 group resulted in substantial hair cell loss compared with the AST/CDDP group and the ML385-only group in mouse cochlear explants (Fig. 3A). Here, these results confirm our hypothesis that AST could interacted with KEAP1 leading the activation NRF2 which helps AST enhance protection against cisplatin-induced ototoxicity.

It was discovered that NRF2 expression and nuclear translocation was reduced following cisplatin exposure for 24 h[49]. The expression of nuclear NRF2 was mainly contributed to the total NRF2 level in HEI-OC1 cell lines following 30 μmol/L cisplatin with or without 50 μmol/L tert-butylhydroquinone pre-treatment for 48 h[49]. Tert-Butylhydroquinone (a valid NRF2 activator) is an electrophilic compound similar with AST[27]. Moreover, the reduction of NRF2 expression and nuclear translocation was observed in ebselen compound for protection against cisplatin ototoxicity in HEI-OC1 cell lines[50]. In our study, the levels of Nrf2 downstream genes including Homx1 and Nqo1 were up-regulated in HEI-OC1 cell lines and cochlear explants following cisplatin treatment with astaxanthine pretreatment. These results supported that NRF2 translocation activated the ARE downstream genes in HEI-OC1 cell lines after exposing to cisplatin with astaxanthine pretreatment. Thus, it was postulated that the changes in total NRF2 level mainly might result from the changes in nuclear NRF2 level. Additionally, a time course of NRF2 level made to reflect the real protective effect. Additionally, a time course of NRF2 level including cytosolic and nuclear may reflect the dynamic protective effect of astaxanthine. Further studies are needed to provide more convincing evidence of astaxanthine binding to KEAP1, as well as the NRF2 changes at different time points.

Accumulated evidence had proven that ROS has an important role in the pathogenesis of cisplatin-induced ototoxicity[51−54]. Characterization of cisplatin-induced cell death in HEI-OC1 cells showed that the induction of apoptosis was aggravated by increased ROS and mitochondrial dysfunction[55,56]. In our study, we used the ROS-sensitive fluorescence indicator DCFH-DA to determine whether AST could attenuate cisplatin-induced ROS after cisplatin treatment. It was shown that AST had favorable properties and strongly reduced ROS generation in HEI-OC1 cells and live cochlear explants following cisplatin treatment. In addition, MTRC staining suggested that AST successfully reversed the decrease in MMP induced by cisplatin in HEI-OC1 cells and live cochlear explants. Our subsequent quantitative analysis of TUNEL and cleaved caspase-3 staining in cochlear explants treated with cisplatin revealed typical characteristics of apoptosis (Fig. 6C and D). In our present study, cisplatin elicited apoptosis both in intrinsic and extrinsic pathways, as evidenced by the increased levels of Fadd, caspase-3, caspase-8, caspase-9, and Bax, as well as the decreased protein level of Bcl-2 that represses apoptosis by blocking Bax. These results were consistent with findings from previous studies[57,58]. Encouragingly, AST attenuated the immunofluorescent staining for apoptosis and mRNA and protein levels of the pro-apoptotic markers mentioned

above in the intrinsic and extrinsic pathways, consequently inhibiting apoptosis and preserving hair cells and HEI-OC1 cells after cisplatin exposure.

Base on protection against cisplatin-induced ototoxicity *in vitro*, the protection of AST in mouse model with CIHL need to be explored before its clinical application. Here, we modified an optimized mouse model of cisplatin ototoxicity to minimize health risks and mortality and offer a cisplatin lesion that is consistent with clinical observations regarding its frequency-specific pattern of damage and severity of toxicity[59,60]. In this study, we used a two-cycle low-dose cisplatin regimen (4 mg/kg) that incorporates a 4-day recovery period between 3-day injection periods in mice to test the protection of AST against CIHL. It was shown that modified cisplatin-treated mice presented as high-frequency hearing loss, which was consistent with clinical reports of progressive hearing loss in humans treated with cisplatin. Altogether, our findings demonstrated that AST could be generalized to the mice and be used as a potential method to protect hearing loss from cisplatin. Additionally, our evidence suggests that AST does not directly interfere with cisplatin in tumor cells, which makes it superior to other therapeutic candidates in clinical trials for protection against cisplatin ototoxicity.

5. Conclusions

For the first time, we discovered that AST firmly bonded with KEAP1 *via* computer molecular simulation, and confirmed that AST protected against cisplatin-induced ototoxicity *via* NRF2-mediated pathway and CIHL. This study demonstrates that AST is a candidate therapeutic agent for CIHL.

Acknowledgments

Author contributions

Benyu Nan and Xi Gu conceived and designed the experiments. Huawei Li and Xinsheng Huang coordinated the research. Benyu Nan performed the experiments and Zirui Zhao and Kanglun Jiang assisted with the experiments. Benyu Nan and Xi Gu wrote and reviewed the manuscript. All authors read and approved the final manuscript.

Conflicts of interest

The authors have declared that no competing interest exists.

Appendix A. Supporting information

Supporting data to this article can be found online at https://doi.org/10.1016/j.apsb.2021.07.002.

References

1. Wu X, Ivanchenko MV, Al Jandal H, Cicconet M, Indzhykulian AA, Corey DP. PKHD1L1 is a coat protein of hair-cell stereocilia and is required for normal hearing. *Nat Commun* 2019;**10**:3801.
2. Muller U, Barr-Gillespie PG. New treatment options for hearing loss. *Nat Rev Drug Discov* 2015;**14**:346−65.
3. Langer T, am Zehnhoff-Dinnesen A, Radtke S, Meitert J, Zolk O. Understanding platinum-induced ototoxicity. *Trends Pharmacol Sci* 2013;**34**:458−69.
4. Frisina RD, Wheeler HE, Fossa SD, Kerns SL, Fung C, Sesso HD, et al. Comprehensive audiometric analysis of hearing impairment and tinnitus after cisplatin-based chemotherapy in survivors of adult-onset cancer. *J Clin Oncol* 2016;**34**:2712−20.
5. Knight KR, Kraemer DF, Neuwelt EA. Ototoxicity in children receiving platinum chemotherapy: underestimating a commonly occurring toxicity that may influence academic and social development. *J Clin Oncol* 2005;**23**:8588−96.
6. Brooks B, Knight K. Ototoxicity monitoring in children treated with platinum chemotherapy. *Int J Audiol* 2018;**57**:S34−40.
7. Anniko M, Sobin A. Cisplatin: evaluation of its ototoxic potential. *Am J Otolaryngol* 1986;**7**:276−93.
8. van Ruijven MW, de Groot JC, Klis SF, Smoorenburg GF. The cochlear targets of cisplatin: an electrophysiological and morphological time-sequence study. *Hear Res* 2005;**205**:241−8.
9. Breglio AM, Rusheen AE, Shide ED, Fernandez KA, Spielbauer KK, McLachlin KM, et al. Cisplatin is retained in the cochlea indefinitely following chemotherapy. *Nat Commun* 2017;**8**:1654.
10. Ciarimboli G, Deuster D, Knief A, Sperling M, Holtkamp M, Edemir B, et al. Organic cation transporter 2 mediates cisplatin-induced oto- and nephrotoxicity and is a target for protective interventions. *Am J Pathol* 2010;**176**:1169−80.
11. More SS, Akil O, Ianculescu AG, Geier EG, Lustig LR, Giacomini KM. Role of the copper transporter, CTR1, in platinum-induced ototoxicity. *J Neurosci* 2010;**30**:9500−9.
12. Thomas AJ, Hailey DW, Stawicki TM, Wu P, Coffin AB, Rubel EW, et al. Functional mechanotransduction is required for cisplatin-induced hair cell death in the zebrafish lateral line. *J Neurosci* 2013;**33**:4405−14.
13. Sheth S, Mukherjea D, Rybak LP, Ramkumar V. Mechanisms of cisplatin-induced ototoxicity and otoprotection. *Front Cell Neurosci* 2017;**11**:338.
14. Gentilin E, Simoni E, Candito M, Cazzador D, Astolfi L. Cisplatin-induced ototoxicity: updates on molecular targets. *Trends Mol Med* 2019;**25**:1123−32.
15. Davinelli S, Nielsen ME, Scapagnini G. Astaxanthin in skin health, repair, and disease: a comprehensive review. *Nutrients* 2018;**10**:1−12.
16. Ambati RR, Phang SM, Ravi S, Aswathanarayana RG. Astaxanthin: sources, extraction, stability, biological activities and its commercial applications—a review. *Mar Drugs* 2014;**12**:128−52.
17. Hussein G, Sankawa U, Goto H, Matsumoto K, Watanabe H. Astaxanthin, a carotenoid with potential in human health and nutrition. *J Nat Prod* 2006;**69**:443−9.
18. Wolf AM, Asoh S, Hiranuma H, Ohsawa I, Iio K, Satou A, et al. Astaxanthin protects mitochondrial redox state and functional integrity against oxidative stress. *J Nutr Biochem* 2010;**21**:381−9.
19. Takemoto Y, Hirose Y, Sugahara K, Hashimoto M, Hara H, Yamashita H. Protective effect of an astaxanthin nanoemulsion against neomycin-induced hair-cell damage in zebrafish. *Auris Nasus Larynx* 2018;**45**:20−5.
20. Kinal ME, Tatlipinar A, Uzun S, Keskin S, Tekdemir E, Ozbeyli D, et al. Investigation of astaxanthin effect on cisplatin ototoxicity in rats by using otoacoustic emission, total antioxidant capacity, and histopathological methods. *Ear Nose Throat J* 2019;**100**:198−205.
21. Niu T, Xuan R, Jiang L, Wu W, Zhen Z, Song Y, et al. Astaxanthin induces the NRF2/HO-1 antioxidant pathway in human umbilical vein endothelial cells by generating trace amounts of ROS. *J Agric Food Chem* 2018;**66**:1551−9.

22. Gu J, Chen Y, Tong L, Wang X, Yu D, Wu H. Astaxanthin-loaded polymer−lipid hybrid nanoparticles (ATX-LPN): assessment of potential otoprotective effects. *J Nanobiotechnol* 2020;**18**:53.

23. Yuan L, Qu Y, Li Q, An T, Chen Z, Chen Y, et al. Protective effect of astaxanthin against La$_2$O$_3$ nanoparticles induced neurotoxicity by activating PI3K/AKT/NRF2 signaling in mice. *Food Chem Toxicol* 2020;**144**:111582.

24. Smith RE, Tran K, Smith CC, McDonald M, Shejwalkar P, Hara K. The role of the NRF2/ARE antioxidant system in preventing cardiovascular diseases. *Diseases* 2016;**4**:34.

25. Bellezza I, Giambanco I, Minelli A, Donato R. NRF2−KEAP1 signaling in oxidative and reductive stress. *Biochim Biophys Acta Mol Cell Res* 2018;**1865**:721−33.

26. Tonelli C, Chio IIC, Tuveson DA. Transcriptional regulation by NRF2. *Antioxid Redox Signal* 2018;**29**:1727−45.

27. Robledinos-Anton N, Fernandez-Gines R, Manda G, Cuadrado A. Activators and inhibitors of NRF2: a review of their potential for clinical development. *Oxid Med Cell Longev* 2019;**2019**:1−20.

28. Kim SJ, Ho Hur J, Park C, Kim HJ, Oh GS, Lee JN, et al. Bucillamine prevents cisplatin-induced ototoxicity through induction of glutathione and antioxidant genes. *Exp Mol Med* 2015;**47**:e142.

29. Ma W, Hu J, Cheng Y, Wang J, Zhang X, Xu M. Ginkgolide B protects against cisplatin-induced ototoxicity: enhancement of Akt−NRF2−HO-1 signaling and reduction of NADPH oxidase. *Canc Chemother Pharmacol* 2015;**75**:949−59.

30. Zhou H, Wang C, Ye J, Chen H, Tao R. Design, virtual screening, molecular docking and molecular dynamics studies of novel urushiol derivatives as potential HDAC2 selective inhibitors. *Gene* 2017;**637**:63−71.

31. Wang B, Feig M, Cukier RI, Burton ZF. Computational simulation strategies for analysis of multisubunit RNA polymerases. *Chem Rev* 2013;**113**:8546−66.

32. Huang D, Li X, Wei Y, Xiu Z. A novel series of l-2-benzyloxycarbonylamino-8-(2-pyridyl)-disulfidyloctanoic acid derivatives as histone deacetylase inhibitors: design, synthesis and molecular modeling study. *Eur J Med Chem* 2012;**52**:111−22.

33. Wu Q, Zhang XS, Wang HD, Zhang X, Yu Q, Li W, et al. Astaxanthin activates nuclear factor erythroid-related factor 2 and the antioxidant responsive element (NRF2−ARE) pathway in the brain after subarachnoid hemorrhage in rats and attenuates early brain injury. *Mar Drugs* 2014;**12**:6125−41.

34. Rao AV, Rao LG. Carotenoids and human health. *Pharmacol Res* 2007;**55**:207−16.

35. Salentin S, Schreiber S, Haupt VJ, Adasme MF, Schroeder M. PLIP: fully automated protein−ligand interaction profiler. *Nucleic Acids Res* 2015;**43**:W443−7.

36. Kumar A, Rajendran V, Sethumadhavan R, Purohit R. Molecular dynamic simulation reveals damaging impact of RAC1 F28L mutation in the switch I region. *PLoS One* 2013;**8**:e77453.

37. Sahihi M, Ghayeb Y. An investigation of molecular dynamics simulation and molecular docking: interaction of citrus flavonoids and bovine beta-lactoglobulin in focus. *Comput Biol Med* 2014;**51**:44−50.

38. Murillo-Cuesta S, Vallecillo N, Cediel R, Celaya AM, Lassaletta L, Varela-Nieto I, et al. A comparative study of drug delivery methods targeted to the mouse inner ear: bullostomy versus transtympanic injection. *J Vis Exp* 2017;**121**:1−11.

39. Block KI, Koch AC, Mead MN, Tothy PK, Newman RA, Gyllenhaal C. Impact of antioxidant supplementation on chemotherapeutic toxicity: a systematic review of the evidence from randomized controlled trials. *Int J Canc* 2008;**123**:1227−39.

40. Freyer DR, Brock P, Knight K, Reaman G, Cabral S, Robinson PD, et al. Interventions for cisplatin-induced hearing loss in children and adolescents with cancer. *Lancet Child Adolesc Health* 2019;**3**:578−84.

41. Haugnes HS, Stenklev NC, Brydoy M, Dahl O, Wilsgaard T, Laukli E, et al. Hearing loss before and after cisplatin-based chemotherapy in testicular cancer survivors: a longitudinal study. *Acta Oncol* 2018;**57**:1075−83.

42. Karasawa T, Steyger PS. An integrated view of cisplatin-induced nephrotoxicity and ototoxicity. *Toxicol Lett* 2015;**237**:219−27.

43. Huang HC, Nguyen T, Pickett CB. Phosphorylation of NRF2 at Ser-40 by protein kinase C regulates antioxidant response element-mediated transcription. *J Biol Chem* 2002;**277**:42769−74.

44. Lee JM, Li J, Johnson DA, Stein TD, Kraft AD, Calkins MJ, et al. NRF2, a multi-organ protector?. *FASEB J* 2005;**19**:1061−6.

45. Guo X, Bai X, Li L, Li J, Wang H. Forskolin protects against cisplatin-induced ototoxicity by inhibiting apoptosis and ROS production. *Biomed Pharmacother* 2018;**99**:530−6.

46. Youn CK, Jo ER, Sim JH, Cho SI. Peanut sprout extract attenuates cisplatin-induced ototoxicity by induction of the Akt/NRF2-mediated redox pathway. *Int J Pediatr Otorhinolaryngol* 2017;**92**:61−6.

47. Deshmukh P, Unni S, Krishnappa G, Padmanabhan B. The KEAP1−NRF2 pathway: promising therapeutic target to counteract ROS-mediated damage in cancers and neurodegenerative diseases. *Biophys Rev* 2017;**9**:41−56.

48. Zhong M, Lynch A, Muellers SN, Jehle S, Luo L, Hall DR, et al. Interaction energetics and druggability of the protein−protein interaction between Kelch-like ECH-associated protein 1 (keap1) and nuclear factor erythroid 2 like 2 (NRF2). *Biochemistry* 2020;**59**:563−81.

49. Zhang W, Xiong H, Pang J, Su Z, Lai L, Lin H, et al. Nrf2 activation protects auditory hair cells from cisplatin-induced ototoxicity independent on mitochondrial ROS production. *Toxicol Lett* 2020;**331**:1−10.

50. Kim SJ, Park C, Han AL, Youn MJ, Lee JH, Kim Y, et al. Ebselen attenuates cisplatin-induced ROS generation through Nrf2 activation in auditory cells. *Hear Res* 2009;**251**:70−82.

51. Rabik CA, Dolan ME. Molecular mechanisms of resistance and toxicity associated with platinating agents. *Cancer Treat Rev* 2007;**33**:9−23.

52. Rybak LP, Mukherjea D, Ramkumar V. Mechanisms of cisplatin-induced ototoxicity and prevention. *Semin Hear* 2019;**40**:197−204.

53. Yakovlev AG, Faden AI. Caspase-dependent apoptotic pathways in CNS injury. *Mol Neurobiol* 2001;**24**:131−44.

54. Sergi B, Ferraresi A, Troiani D, Paludetti G, Fetoni AR. Cisplatin ototoxicity in the Guinea pig: vestibular and cochlear damage. *Hear Res* 2003;**182**:56−64.

55. So HS, Kim HJ, Lee JH, Lee JH, Park SY, Park C, et al. Flunarizine induces NRF2-mediated transcriptional activation of heme oxygenase-1 in protection of auditory cells from cisplatin. *Cell Death Differ* 2006;**13**:1763−75.

56. So H, Kim H, Kim Y, Kim E, Pae HO, Chung HT, et al. Evidence that cisplatin-induced auditory damage is attenuated by downregulation of pro-inflammatory cytokines *via* NRF2/HO-1. *J Assoc Res Otolaryngol* 2008;**9**:290−306.

57. Li Y, Li A, Wu J, He Y, Yu H, Chai R, et al. MiR-182-5p protects inner ear hair cells from cisplatin-induced apoptosis by inhibiting FOXO3a. *Cell Death Dis* 2016;**7**:e2362.

58. Borse V, Al Aameri RFH, Sheehan K, Sheth S, Kaur T, Mukherjea D, et al. Epigallocatechin-3-gallate, a prototypic chemopreventive agent for protection against cisplatin-based ototoxicity. *Cell Death Dis* 2017;**8**:e2921.

59. Fernandez K, Wafa T, Fitzgerald TS, Cunningham LL. An optimized, clinically relevant mouse model of cisplatin-induced ototoxicity. *Hear Res* 2019;**375**:66−74.

60. Park HJ, Kim MJ, Rothenberger C, Kumar A, Sampson EM, Ding D, et al. GSTA4 mediates reduction of cisplatin ototoxicity in female mice. *Nat Commun* 2019;**10**:1−14.